Research Article | Vol. 32, No. 20 / 23 Sep 2024 / Optics Express 35462
Optics EXPRESS

Mid-infrared ultrafast soliton molecules from a few-cycle Cr:ZnS laser

XIYUE ZHANG,[1,2] YUCHEN WANG,[1,8] WEIBO WU,[1,3] TINGHUI AN,[1,4] YIGUANG JIANG,[1] JINTAI FAN,[1,9] BENXUE JIANG,[5] PINGHUA TANG,[3,10] GIANLUCA GALZERANO,[6] PAOLO LAPORTA,[6,7] AND LONG ZHANG[1]

[1]*Shanghai Institute of Optics and Fine Mechanics, Chinese Academy of Sciences, Shanghai 201800, China*
[2]*University of Chinese Academy of Sciences, Beijing 100049, China*
[3]*School of Physics and Optoelectronics, Xiangtan University, Xiangtan 411105, China*
[4]*ShanghaiTech University, Shanghai 200120, China*
[5]*School of Physics Science and Engineering, Tongji University, Shanghai 200092, China*
[6]*Istituto di Fotonica e Nanotecnologie, Consiglio Nazionale delle Ricerche, Milano 20133, Italy*
[7]*Dipartimento di Fisica, Politecnico di Milano, Milano 20133, Italy*
[8]*wangyuchen@siom.ac.cn*
[9]*jtfan@siom.ac.cn*
[10]*pinghuatang@xtu.edu.cn*

Abstract: Soliton molecules, or soliton bound states, are envisioned to make far-reaching changes in both fundamental research and applications. Here, we report on the generation and precision manipulation of soliton molecules based on a Kerr-lens mode-locked single-crystal Cr:ZnS laser at 2.4 μm. In the classical soliton regime, self-starting near-transform-limited pulses with a duration of 37 fs, less than 5 optical cycles, have been obtained at a repetition frequency of 173 MHz and an average output power of 572 mW. By fine-tuning the cavity group-delay dispersion profile, bi-soliton states with pulse durations between 55 fs and 98 fs with temporal separations between 348 fs and 604 fs have been observed and characterized. These are the shortest pulse duration and separation of soliton molecules reported so far in the mid-infrared region, to the best of our knowledge. With the ability of precision manipulation of soliton molecules generated on a sub-100-fs timescale, the tunable mid-infrared soliton molecule source paves the way for applications in the fields of telecommunications and ultrafast laser technologies.

1. Introduction

Solitons, as a peculiar case of self-sustaining wave packages, have been found in many fields of study such as fluid mechanics, plasmas and nonlinear optical systems [1–3]. Optical solitons, like solitons in other media, are subjected to interactions including attraction, repulsion or collision [2,4,5]. Optical solitons generated from passively mode-locked lasers are the result of the intricate double-balance between dispersion and nonlinearity, gain and losses [6,7] often described by the Ginzburg-Landau equation (GLE) [8]. Multiple optical solitons may form a variety of bound states through interaction, often referred to as optical solitons molecules [4,6,9]. Soliton molecules have attracted increasing attention not only as an optimal subject for the study of soliton dynamics [1,10], also as an analogy to chemical molecules [9,11] and for their potential for telecommunication [12].

Being central to the research on soliton molecules, their generation, manipulation and detection have seen an overwhelming surge of research endeavors. As an effective platform for the generation of optical solitons, fiber lasers have been the primary choice of laser resonator in which diverse types of multi-soliton states were theoretically predicted and experimentally demonstrated, including compound states of solitons, bright/dark soliton states and vector soliton

#537071 https://doi.org/10.1364/OE.537071
Journal © 2024 Received 7 Aug 2024; revised 9 Sep 2024; accepted 10 Sep 2024; published 17 Sep 2024

Optics EXPRESS

states [6,13–17]. So far, tightly and loosely bound soliton molecules have been discovered, which are generated owning to the varying binding strength between neighboring soliton molecules [9,18–22]. In previous studies, it has been shown that when two solitons are close to each other but in opposite phases, a stable equilibrium point establishes at the crossing between the attractive interaction and the repulsive interaction [23]. In fact, the time separation between solitons, as a key factor in determining the intermolecular force of solitons, leads to different soliton molecular states and intermolecular interactions. Therefore, the time separation and relative phase control of bound state solitons play a fundamental role in various optical applications based on soliton molecules [20].

In addition to fiber lasers, multi-pulse operations have also been observed in bulk lasers such as Ti^{3+}:Sapphire [24–26] by changing the cavity configuration or controlling the pumping power [27]. Often referred to as "Ti^{3+}:Sapphire of the mid-infrared (mid-IR)", Cr^{2+}:ZnS/ZnSe are proven to be an excellent platform for mid-IR ultrafast lasers [28], as passively mode-locked laser operation using this class of gain media was achieved with different types of saturable absorbers [29–32] and recently down to the few-optical cycle regime [33–35].

According to Kalashnikov *et al.* [36], with both sufficiently high third-order nonlinearity as well as emission and absorption cross section, Cr:ZnS/ZnSe is also an unique platform for studying multi-pulse interactions in the few-cycle regime [37,38]. Recently, several studies on the generation of bound soliton molecules have reported based on Cr:ZnS/ZnSe. Bi-soliton states and multi-soliton states have been reportedly generated from Kerr-lens mode-locked (KLM) [32] and semiconductor saturable absorber mirror mode-locked Cr:ZnS/ZnSe lasers [39,40], but with limited means of control, leading to typically loosely-bound solitons with pulse-to-pulse temporal separation from hundreds of femtoseconds to few picoseconds [32,39].

In this work, we report an in-depth investigation on the generation and the manipulation of soliton and bi-soliton states based on a dispersion fine-tuned KLM Cr:ZnS resonator. The passively mode-locked pulse train, operating in the classical soliton mode-locking regime, is obtained at a pulse duration of 37 fs, a repetition rate of 173 MHz and an average output power of 572 mW. Tightly-bound bi-soliton states, or soliton molecules, were generated and controlled by the discrete tuning of the intracavity dispersion. The soliton molecules are characterized by sub-100-fs pulse durations at variable relative phase relations and a tunable intramolecular separation, which can be interpreted as a tunable interaction strength of the soliton molecule.

2. Theoretical description of the interactions of soliton molecules

For nonlinear dissipative systems, the complex cubic–quintic Ginzburg-Landau equation (CGLE), as a generalization of the higher order dissipation terms in the nonlinear Schrödinger equation, can be used to describe a variety of soliton propagation processes including soliton molecular pulses, in particular for the representation of a laser containing dispersion, nonlinearity, gain and losses. The normalized form can be written as [6,41]:

$$i\psi_z + D\psi_{tt}/2 + |\psi^2|\psi + \nu|\psi^4|\psi = i\delta\psi + i\varepsilon|\psi^2|\psi + i\beta\psi_{tt} + i\mu|\psi^4|\psi \tag{1}$$

where ψ is the envelope of the field, t is the retarded time, z is the normalized propagation distance along the cavity, ψ_z is the first-order z-derivative and ψ_{tt} is the second-order t-derivative. D is the group velocity dispersion coefficient, δ is the linear gain (>0) or loss (<0) coefficient. Furthermore, i$\beta\psi_{tt}$ accounts for spectral filtering (β>0), $\varepsilon|\psi^2|$ represents the nonlinear gain absorption, μ represents a higher-order correction to the nonlinear absorption, and ν corresponds to a possible higher-order correction term to the intensity-dependent refractive index. For stable local solutions of CGLE, we call them solitons. Soliton solutions need to satisfy the composite balance of dispersion and nonlinearity, gain and loss, as shown in Fig. 1(a).

Optics EXPRESS

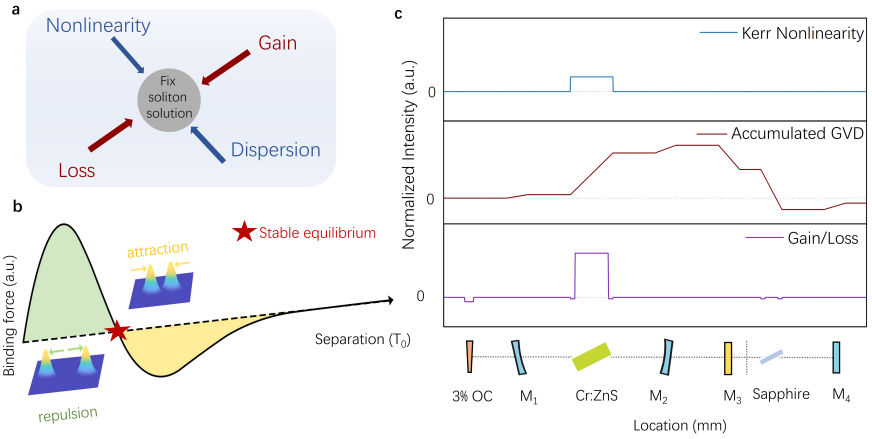

Fig. 1. (a) Soliton solutions in dissipative systems, the composite balance between several effects including nonlinearity, dispersion, loss and gain. (b) Illustration of the interactions of anti-phase soliton molecule at different pulse separations. (c) Distribution of nonlinearity, dispersion, loss and gain throughout the linear resonator.

For soliton solutions satisfying the CGLE equation, the evolution of solitons can be expressed as:

$$\psi(t,z) = \psi_0(t-\rho/2) + \psi_0(t+\rho/2)e^{i\phi} \tag{2}$$

which indicates that in the process of two solitons interaction, basically only the two parameters of pulse separation ρ and relative phase difference ϕ change [42].

For soliton molecules with a certain phase relationship, in particular when their phase difference is π (anti-phase), there is a balance between attractive and repulsive forces established through the Kerr nonlinearity of an optical medium in which the solitons traverse [23]. When the soliton molecules are in a repulsive interaction, the pulses repel each other. Similarly, the attraction corresponds to the mutual attraction of the pulses. When the soliton molecules are in quadrature phase, the intermolecular force remains zero at all separations (Fig. 1(b)). Intermolecular forces can be expressed as [23]:

$$\frac{d}{d\zeta}\langle\omega\rangle|_{envelope} = -\frac{1}{W}\int_{-\infty}^{\infty}\frac{\partial}{\partial\tau}(|u+v|^2)d\tau \tag{3}$$

where ζ is the propagation distance, $\langle\omega\rangle$ is the average soliton frequency, W is the soliton energy, time τ is normalized to the 1/e half width of the launched pulse, T_0, u and v represent the fields of the two pulses. The relative phase information of the pulse can be obtained from the spectrum of a periodic train of solitons. In general, the intensity of the spectral center depends on the phase difference between bound soliton pairs. Both the 0-phase and pai phase bound solitons have spectral symmetry. The difference is that the 0-phase bound solitons have the smallest spectral center, while the π-phase bound solitons have the largest spectral center. The spectra of $\pi/2$ phase and -$\pi/2$-phase bound soliton pairs show obvious asymmetric characteristics. A notable feature of $\pi/2$ bound solitons is that the left peak of the spectrum is larger than the right peak, while the -$\pi/2$ bound solitons exhibit the opposite characteristic [43–45]. Specifically, the phase difference $(0, \pm\pi/2, \pi)$ between the two pulses can be obtained from the spectrum using this relation [45,46]:

$$\phi = 2\pi(\omega_0-\omega_1)/(\omega_2-\omega_1) \tag{4}$$

where ω_0 is the center frequency of the fitting sech^2 curve, and ω_1 and ω_2 are the frequencies closest to ω_0.

Optics EXPRESS

Based on the CGLE theoretical model, the distribution of Kerr nonlinearity, accumulated group velocity dispersion (GVD), gain and loss throughout an unfolded linear laser resonator is qualitatively represented in Fig. 1(c). The Kerr nonlinearity of the cavity is mainly attributed to the Cr:ZnS single crystal where locates the beam waist. The GVD accumulates over multiple reflections on the low-dispersion high-reflectivity (HR) mirrors, the optical path through gain media Cr:ZnS, the chirped mirrors and a sapphire plate. In addition, the gain in the cavity is mainly arose from the gain media Cr:ZnS. Moreover, the intracavity losses are mainly due to the output coupler (OC) and interfaces of the Cr:ZnS crystal and the sapphire plate put at imperfect Brewster's angles.

In order to limit the strength of intra-cavity second-order nonlinear interactions leading to randomly quasi-phase-matched second-harmonic generation and difference frequency generation often observed when using polycrystalline Cr:ZnS/ZnSe gain media [47]. These nonlinear frequency conversion may lead to a further dissipation of the intracavity soliton energy and complications of the physical picture. As a result, we have selected the single-crystalline Cr:ZnS as the gain medium in this work.

3. KLM laser resonator and the soliton mode-locking

As shown in Fig. 2(a), a KLM Cr:ZnS cavity is constructed using five dielectric mirrors: two plano-concave HR mirrors M_1 and M_2 with ROC = −100 mm, a plane chirped mirror M_3, a plane HR mirror M_4 and a wedged OC. The three cavity HR mirrors M_1,M_2 and M_4 have a reflectance R>99.5% from 2000 to 2800 nm, a R<5% from 1500 to 1650 nm, a group delay dispersion |GDD|<100 fs^2 from 2100 to 2500 nm (custom-made by Qifeng Landa Co. Ltd). M_3 has a reflectance R>99.5% from 1700 to 2700 nm and a nominal GDD = −250 fs^2 (Ultrafast Innovations GmbH). The OC has a reflectance R = 97% from 2100 to 2400 nm (LAYERTEC GmbH). The total length of the cavity is 0.86 m, with the asymmetric HR arm and OC arm length ratio of 3:5. A 5-mm-long Cr:ZnS single crystal (Miracrys), with a doping level of 1 × 10^{19} ions/cm^3, is used as the gain medium in this experiment, positioned at the Brewster's angle between plano-concave mirrors. The crystal is mounted by a copper heat sink, which is controlled at 20 °C by a Peltier electric-cooler and a temperature controller.

The pump source is a single-mode narrow-linewidth linearly-polarized CW Er-doped fiber laser (CONNET, VFLS-1550-B-MP) with a maximum output power of 15 W and an operating wavelength of 1550 nm. Using a plano-convex lens with focal length of 100 mm, the pump laser is focused on Cr:ZnS crystal through the plano-concave mirror. The designed spot size of the pump mode is slightly smaller than the fundamental mode of the resonator to facilitate the soft-aperture KLM, as calculated by the standard ABCD matrix method (ReZonator) [35].

The dispersion profiles of the intracavity components including the gain element, the 2-mm thick sapphire plate (calculated using the standard Sellmeier equations) and the chirped mirror (provided by the suppliers) are shown in Fig. 2(b). Two reflections on the chirped mirror and a 2 mm-thicked sapphire (Dien Tech Ltd.) are used to compensate for the positive dispersion of the Cr:ZnS crystal. In fact, the atmospheric humidity will have a greater impact on the dispersion of the cavity, therefore atmospheric dispersion is also taken into account in the GDD curves (at 40% relative humidity) [48,49]. As a result, the net round-trip GDD at the central wavelength of the laser output (~2.4 μm) is estimated to be −252 fs^2.

The laser efficiency has been characterized as shown in Fig. 2(c) by measuring pump powers before the plano-concave input-coupling mirror and the output power from the OC. Under continuous-wave conditions, when the incident pump power is 9 W, the maximum output power of the Cr:ZnS laser is 0.83 W. After optimizing the continuous wave output power and crystal position, the self-starting KLM is realized. When the incident pump power is greater than 3 W, the self-starting KLM state can be achieved by adjusting the cavity alignment properly. When the pump power is 7 W, the maximum average output power of soliton mode-locking is 572 mW.

Optics EXPRESS

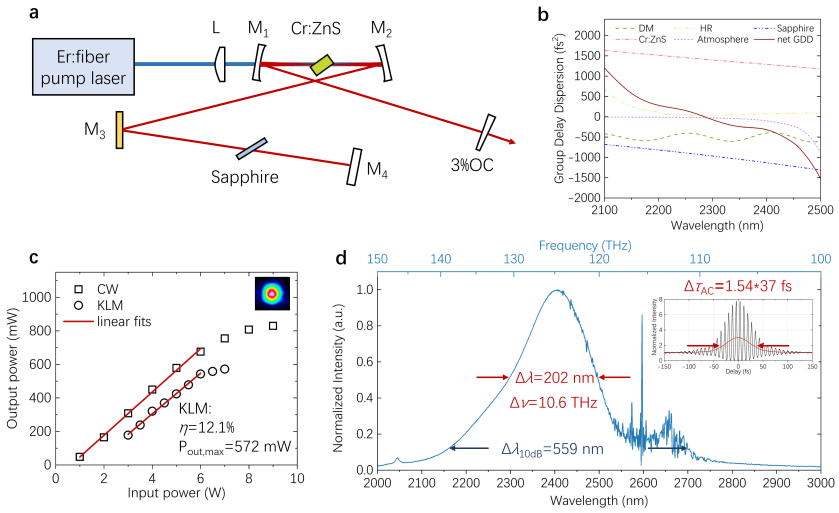

Fig. 2. (a) Astigmatism-compensated asymmetric linear cavity configuration. L: lens, f=100 mm; M1, M2: HR mirrors with a radius of curvature (ROC)=100 mm; M3: HR dispersion mirror; M4: HR mirrors; OC: Zero dispersion output coupler mirror. (b) GDD spectra of the resonator elements and the net GDD of the cavity. The GDD of the HR mirror is the sum GDD of five reflections. (c) Output power versus incident pump power in both CW and KLM regimes. Inset is the beam quality of the oscillator. Spectrum (d) and interferometric autocorrelation (Inset) of the 173 MHz pulse trains generated by the KLM Cr:ZnS.

Insert in Fig. 2(a) illustrates the laser spot profile measured extra-cavity at a distance of 50 cm from the OC using a mid-IR beam profiler (DataRay S-WCD-IR-BB-7.5). The laser beam quality is characterized measured by the mid-IR beam profiler in the mode-locking operation regime to M^2_x and M^2_y are 1.08 and 1.06, respectively (as shown Fig. S1 in Supporting Information(SI)).

The output pulse spectrum is measured by a Fourier-transform infrared (FTIR) spectrometer (Arcoptix FTIR-L1-120-4TE) as shown in Fig. 2(d). The pulse autocorrelation is measured by a home-made interferometric autocorrelator based on the two-photon absorption in an amplified InGaAs detector (Thorlabs PDA20CS2), with the residual chirp due to the OC compensated by a 0.5 mm thick germanium plate. As can be seen from Fig. 2(d), the output spectrum is characterized by a central wavelength of 2404 nm (124.7 THz), a full width at half maximum (FWHM) bandwidth of 202 nm (10.6 THz). The spectrum is contaminated with near-infrared radiation at wavelengths greater than 2.5 μm at certain levels of water vapor absorption inside the resonator, showing a 10-dB bandwidth of 559 nm. Insert in Fig. 2(d) shows the autocorrelation tracks recorded at 173 MHz repetition and the retrieved intensity autocorrelation profile (red curve). The pulse width is measured to be ~37 fs (corresponding to less than 5 optical cycles), with a time-bandwidth product of 0.39 which is larger than the transform-limited value of 0.315 for $sech^2$-pulses, indicating that there is a small residual chirp. Since the first Kerr lens mode-locking (KLM) operation around 2.4 μm was achieved on Cr:ZnSe/Cr:ZnS lasers, femtosecond pulses with short pulse widths based on KLM have been significantly improved. In case of single soliton operating state, a kerr lens mode-locked Cr:ZnS laser with a pulse width of sub-30-fs has been reported successively [33]. In addition, the current Cr:ZnS oscillator based on the SESAM [29,30], graphene [50] and carbon nanotubes [51] mode-lock have also realized the ultra-short pulse output of sub-100-fs.

The pulse train and its radio-frequency (RF) spectrum is measured using a fast HgCdTe photodetector (~1 GHz bandwidth, from Vigo Systems) combined with an oscilloscope (Tektronix

Optics EXPRESS

MDO34) and an electrical spectrum analyzer (ESA) (Keysight N9020A). Fig. S2(a) shows a resolution bandwidth (RBW) of 3 MHz at a span of 1.5 GHz. The signal-to-noise (SNR) ratio of 38 dB can be measured for the repetition frequency signal at 173 MHz without Q-switching sidebands in the RF spectrum. The SNR further increases to 64 dB by narrowing the resolution bandwidth to 3 kHz, as shown in Fig. S2(b). As shown Fig. S2(c), the pulse train of the oscillator in the soliton mode-locked state displayed good pulse-to-pulse stability. The mode-locked state can last for more than two hours in the laboratory environment without any enclosure for the cavity.

4. Tunable soliton molecules

Tightly-bound bi-soliton states have been found with reproducibility at intracavity round-trip GDDs smaller than -400 fs^2, at a fixed pump power of 4 W. The amount of GDD within the cavity has been discretely adjusted changing the number of bounces on the chirped mirror and the thickness of the sapphire plate. GDD spectra of the resonator elements and the net GDD of the cavity with different soliton states are displayed in Fig. S3. Soliton molecules with pulse separation of 348 fs, 396 fs, 574 fs and 604 fs, pulse duration of 60 fs, 55 fs, 84 fs and 98 fs were obtained, corresponding to multiples of 5.8, 7.2, 6.8 and 6.2 respectively. For the anti-phase soliton molecules, the separation at the stable equilibrium can be expressed as [23]:

$$\rho = k\tau_p \tag{5}$$

where ρ represents a mutual separation, k is a constant and τ_p is the pulse duration. This indicates that there is a relationship between pulse separation and pulse width at the equilibrium point for the anti-phase bi-soliton state, which can also be interpreted as a binding energy factor of the soliton molecule [23]. As a result, in the case of an anti-phase soliton molecule, their mutual stable equilibrium condition can be harnessed for the generation of highly stable soliton molecules which may lead to real world applications.

Generally speaking, ultra-short pulse formation in Kerr-lens mode-locked resonator is mainly the result of the interplay between anormalous GVD and self-phase modulation (SPM). The increase of the SPM produces a stronger nonlinear chirp, with only the center part being compensated by negative GVD, which results in the separation of the sidelobal pulses [25,31] and the subsequent formation of a soliton molecule at equilibrium. Fig. 3 shows the spectrum and pulse autocorrelation of the resonator under different GDD. Interestingly, the phase difference of the bound states are π (Fig. 3(a), (d)), $\pi/2$ (Fig. 3(b)) and $-\pi/2$ (Fig. 3(c)) under different dispersion conditions, indicating that the dispersion condition not only changes the temporal separation between pulse-to-pulse, but also change their relative phase. In this experiment, a tunable factor formed between 5.8 and 7.2, showing a strong direct interaction between the pulses.

An simple field-resolved analytical model of the bi-soliton condition has been built in Matlab. Two pulses with sech^2 pulse envelope at the center frequency as the measured spectra, with given phase and time separations are constructed. The autocorrelation of the analytical model is fitted to the autocorrelations of the pulses (See Fig. S4 for further details), by varying a set of parameters including the pulse durations of the two solitons, the intensity ratio of the two solitons, their temporal separation, their residual chirp etc. Taking the soliton molecular pulse with time separation of 348 fs as an example (Fig. 4(a)). With the parameters including pulse width and time separation, fitting results are in good agreement with the experimental data, as shown in Fig. 4(b). As a result of the fitting, the energy ratio between the two solitons is found to be close to 1. Moreover, the intensity profile and the field profile of the soliton molecule have been reconstructed based on the autocorrelation curve (Fig. S5), the pulse width of the reconstructed solitons is 62 fs (as shown in Fig. 4(c)), with an difference<3% compared to the pulse width retrieved from the interferometric autocorrelation data. This may be due to the

Optics EXPRESS

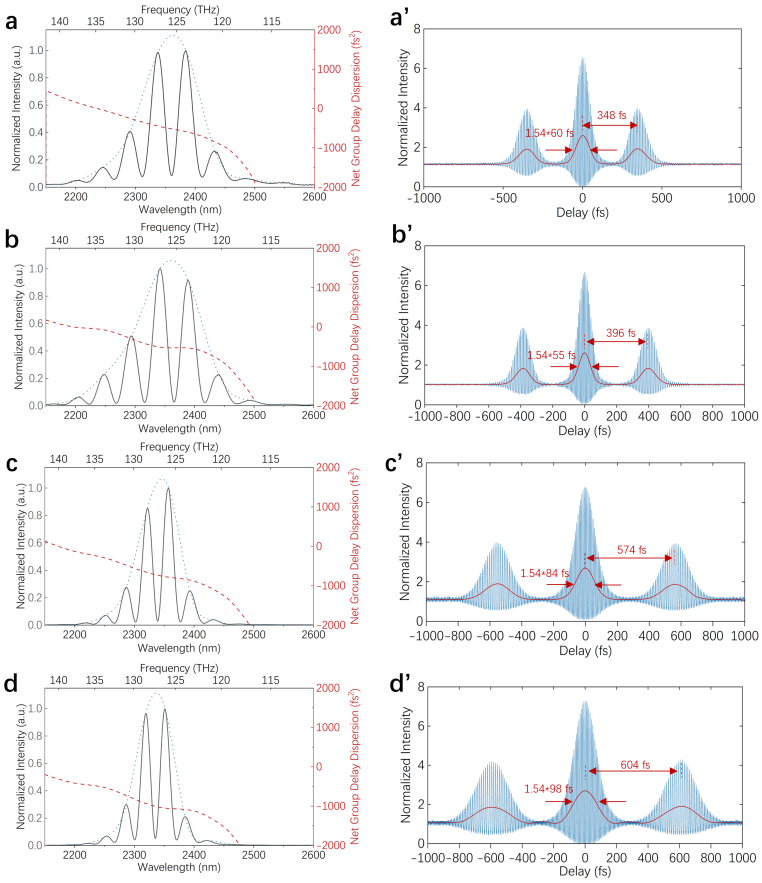

Fig. 3. Spectra, net GDD (left column) and corresponding autocorrelation traces (right column) of the laser output in soliton molecule operation mode. The pulse separations are measured to be (a') 348 fs, (b') 396 fs, (c') 574 fs, and (d') 604 fs, respectively. The red curves in the autocorrelation correspond to the intensity autocorrelation profiles.

insufficient linearity of the translation mechanism (voice coil motor) of the interferometer and the incompleteness of the model.

The time and frequency domain analysis has also been carried out for the soliton molecules when the intracavity GDD is -1035 fs^2. In Fig. 5(a), the RF spectrum of bound solitons are shown, displaying fundamental modelocking at repetition rate of ~173 MHz. As the resolution bandwidth is narrowed from 3 MHz to 3 kHz, the SNR is increased from 34 to 63 dB, indicating good stability in the mode-locked state. The pulse train of soliton molecules is represented in Fig. 5(b). Due to the limitation of bandwidth of the detector (rise time on the level of 1 ns), the temporal profile of the soliton molecule itself cannot be resolved. But these results indicate that the soliton molecule finds itself at an equilibrium state, given the stable repetition frequency signal without any sidebands. In addition, we also measured the polarization state of the soliton molecule. It can be clearly seen in Fig. 5(c) that the bound-state solitons present a linearly polarized state with an extinction ratio of 891.

As can be seen from Fig. 6(a), the bound soliton is more easily generated under large negative dispersion. When the GDD value changes from -1035 fs^2 to 397 fs^2, the spectrum shows a change between bound-state solitons, solitons and finally dissipative solitons. It can be seen from

Optics EXPRESS

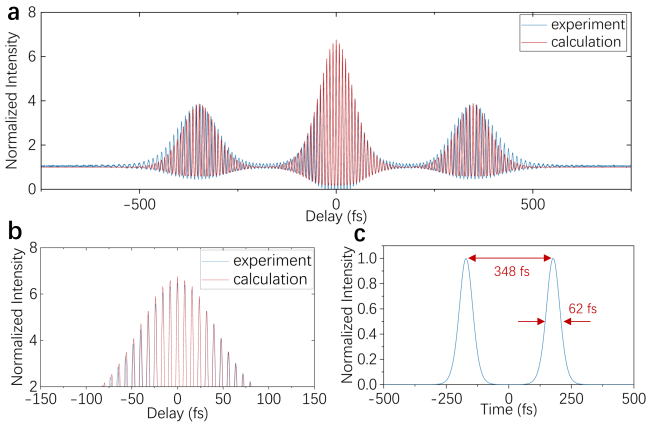

Fig. 4. Autocorrelation traces (a) and partial enlarged detail of the central peak (b) of soliton molecules (blue) with their corresponding fitting results (red). (c) Reconstructed intensity profile of the soliton molecule at a pulse separation of 348 fs.

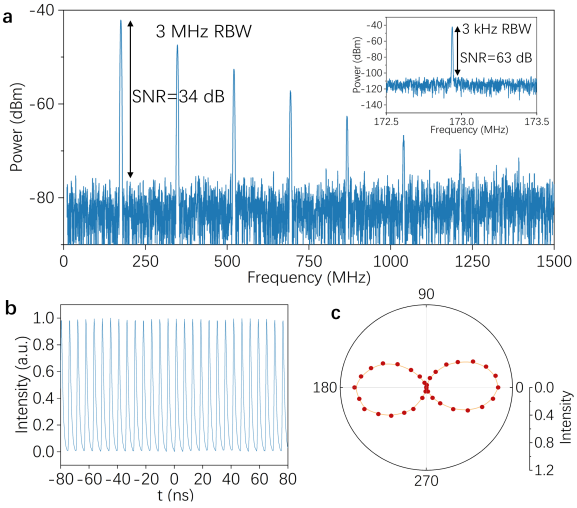

Fig. 5. (a) RF spectrum of the bound-state soliton molecules in a 3 MHz and 3 KHz (Insert) resolution bandwidth. (b) Pulses train of Cr:ZnS laser in soliton molecules mode-locked state. (c) transmittance of the soliton molecules through a rutile Glan-Taylor mid-IR polarizer as a function of its rotation angle θ.

Optics EXPRESS

Fig. 6(b) that a certain range of negative GDD is conducive to pulse splitting. Starting from the larger intracavity GDD, at a fixed pump power of 4 W, the stable mode-locking first develops into a soliton molecule state, and then the pulse interval gradually decreases with the continuous reduction of intracavity GDD, and the soliton mode-locking is restored at a threshold intracavity GDD value. The pulse duration and the average output power of the laser also decreases with the decrease of the dispersion value.

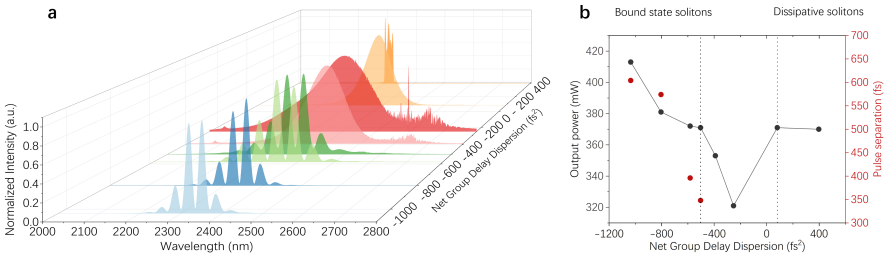

Fig. 6. (a) Output laser spectra with different net GDD, the condition of mode-locking operation varies from soliton molecules to classical solitons and eventually to dissipative solitons. (b) The average output power (black symbol) and pulse separation (red symbol) are functions of the net GDD, with the pulse intervals in the soliton molecules state in parentheses.

At present, bound state solitons in the fiber lasers are observed with pulse separation mostly on the levels of a few ps. The soliton molecules with shorter pulse separation, especially wavelength over 2 μm, are rarely reported (Table 1). Precisely controlled dispersion and further electronic modulation can be used to tailor the temporal separation and phase of ultrafast soliton molecules, promising higher-order coding formats that will further expand the channel capacity of optical transmission [58–60]. Given the possibility of further increasing the pulse repetition rate to GHz level [61], the demonstrated antiphase soliton molecules with tunable binding energies based on KLM Cr:ZnS laser pave ways for ultrahigh large-capacity telecommunication [7], optical switching [19,20], storage [62,63].

Table 1. Mode-locked lasers generating soliton molecules or multiple pulses. λ_0 is the center of wavelength, ρ is the pulse separation, τ_p is the pulse width, $\Delta\phi$ is the phase difference between the bound solitons.

λ_0 (nm)	ρ (fs)	τ_p (fs)	ρ/τ_p	$\Delta\phi$	Ref.
~800	100-1000	-	-	-	Lai *et al.* [24]
~800	98-541	15	6.5-36	0-π	Kitano *et al.* [25]
1035	187000	8200	2.28	-	Ortaç *et al.* [52]
1550	580	82	7.07	π/2	Zou *et al.* [53]
1558	26200	720	36.38	-	Fu *et al.* [54]
1970	4120	1280	3.22	0, π	Ren *et al.* [55]
2000	1800	870	2.06	π	Chernysheva *et al.* [56]
2404	348-604	55-98	5.8-7.2	π, $\pm\pi/2$	This Work
2800	5400-12400	430-805	-	8π, 0.4π	Huang *et al.* [57]

5. Conclusion

In summary, a dispersion fine-tuned KLM single-crystal Cr:ZnS laser at a wavelength of 2.4 μm and a repetition frequency of 173 MHz is implemented. In soliton regime, mode-locked pulse

Optics EXPRESS

train has been generated with a minimum pulse duration of 37 fs, less than 5 optical cycles, at an average output power up to 572 mW, corresponding to a pulse energy of 2.9 nJ. By discretely varying the intracavity dispersion, ultrafast soliton molecules with pulse durations from 55 fs to 98 fs, at pulse separations between the 348 fs and 604 fs have been observed. The generation of few optical cycle mid-IR soliton molecules and their manipulation at a sub-100-fs time scale could pave ways for telecommunication, precision ranging and optical data storage.

Funding. Chinese Academy of Sciences Youth Interdisciplinary Team (JCTD-2022-09); Youth Innovation Promotion Association of the Chinese Academy of Sciences (2022244); Shanghai Pujiang Program (22PJ1414900); Natural Science Foundation of Hunan Province (2023JJ30596); National Key Research and Development Program of China (2021YFB3501700, 2022YFB3605704); Strategic Priority Research Program of the Chinese Academy of Sciences (XDB0650000).

Acknowledgments. The authors would like to thank Toney Fernandez, Jiapeng Huang and Meng Pang for fruitful discussions, Alberto Comin for insights on the numerical calculation of the pulse autocorrelation.

Disclosures. The authors declare no conflicts of interest.

Data availability. The data that support the findings of this study are available within the article and its supporting information.

Supplemental document. See Supplement 1 for supporting content.

References

1. G. I. Stegeman and M. Segev, "Optical spatial solitons and their interactions: Universality and diversity," Science **286**(5444), 1518–1523 (1999).
2. A. Chabchoub, O. Kimmoun, H. Branger, *et al.*, "Experimental observation of dark solitons on the surface of water," Phys. Rev. Lett. **110**(12), 124101 (2013).
3. D. R. Solli, C. Ropers, P. Koonath, *et al.*, "Optical rogue waves," Nature **450**(7172), 1054–1057 (2007).
4. J. Peng and H. Zeng, "Build-up of dissipative optical soliton molecules via diverse soliton interactions," Laser Photonics Rev. **12**(8), 1800009 (2018).
5. J. K. Jang, M. Erkintalo, S. G. Murdoch, *et al.*, "Ultraweak long-range interactions of solitons observed over astronomical distances," Nat. Photonics **7**(8), 657–663 (2013).
6. P. Grelu and N. Akhmediev, "Dissipative solitons for mode-locked lasers," Nat. Photonics **6**(2), 84–92 (2012).
7. Y. Yang, W. Lin, Y. Guo, *et al.*, "Phase-encoding of loosely bound soliton molecules," APL Photonics **9**(3), 031305 (2024).
8. D. Tang, B. Zhao, L. Zhao, *et al.*, "Soliton interaction in a fiber ring laser," Phys. Rev. E **72**(1), 016616 (2005).
9. G. Herink, F. Kurtz, B. Jalali, *et al.*, "Real-time spectral interferometry probes the internal dynamics of femtosecond soliton molecules," Science **356**(6333), 50–54 (2017).
10. Y. Zhao, J. Fan, Y. Song, *et al.*, "Extraction of internal phase motions in femtosecond soliton molecules using an orbital-angular-momentum-resolved method," Photonics Res. **8**(10), 1580–1585 (2020).
11. W. He, M. Pang, D.-H. Yeh, *et al.*, "Synthesis and dissociation of soliton molecules in parallel optical-soliton reactors," Light: Sci. Appl. **10**(1), 120 (2021).
12. O. Melchert, S. Willms, S. Bose, *et al.*, "Soliton molecules with two frequencies," Phys. Rev. Lett. **123**(24), 243905 (2019).
13. W. H. Renninger, A. Chong, and F. W. Wise, "Area theorem and energy quantization for dissipative optical solitons," J. Opt. Soc. Am. B **27**(10), 1978–1982 (2010).
14. K. Krupa, K. Nithyanandan, U. Andral, *et al.*, "Real-time observation of internal motion within ultrafast dissipative optical soliton molecules," Phys. Rev. Lett. **118**(24), 243901 (2017).
15. P. Rohrmann, A. Hause, and F. Mitschke, "Two-soliton and three-soliton molecules in optical fibers," Phys. Rev. A **87**(4), 043834 (2013).
16. X. Hu, J. Guo, G. D. Shao, *et al.*, "Dissipative dark-bright vector solitons in fiber lasers," Phys. Rev. A **101**(6), 063807 (2020).
17. Z. He, Y. Du, Y. Zhang, *et al.*, "Dislocated vector asymmetric soliton molecules in birefringence-managed fiber lasers," Phys. Rev. A **108**(1), 013514 (2023).
18. M. Li, Y. Song, C. Zhang, *et al.*, "Generation and observation of multiple solitons from a mid-infrared ultrafast fiber laser," Chin. Opt. Lett. **22**(3), 031405 (2024).
19. F. Kurtz, C. Ropers, and G. Herink, "Resonant excitation and all-optical switching of femtosecond soliton molecules," Nat. Photonics **14**(1), 9–13 (2020).
20. S. Liu, Y. Cui, E. Karimi, *et al.*, "On-demand harnessing of photonic soliton molecules," Optica **9**(2), 240–250 (2022).
21. D. Tang, W. Man, H. Y. Tam, *et al.*, "Observation of bound states of solitons in a passively mode-locked fiber laser," Phys. Rev. A **64**(3), 033814 (2001).

Optics EXPRESS

22. W. He, M. Pang, D.-H. Yeh, *et al.*, "Formation of optical supramolecular structures in a fibre laser by tailoring long-range soliton interactions," Nat. Commun. **10**(1), 5756 (2019).
23. A. Hause, H. Hartwig, M. Böhm, *et al.*, "Binding mechanism of temporal soliton molecules," Phys. Rev. A **78**(6), 063817 (2008).
24. M. Lai, J. Nicholson, and W. Rudolph, "Multiple pulse operation of a femtosecond ti: sapphire laser," Opt. Commun. **142**(1-3), 45–49 (1997).
25. H. Kitano and S. Kinoshita, "Stable multipulse generation from a self-mode-locked ti: sapphire laser," Opt. Commun. **157**(1-6), 128–134 (1998).
26. M. Lederer, B. Luther-Davies, H. Tan, *et al.*, "Multipulse operation of a ti: sapphire laser mode locked by an ion-implanted semiconductor saturable-absorber mirror," J. Opt. Soc. Am. B **16**(6), 895–904 (1999).
27. X. Han, J. Wu, and H. Zeng, "Controllable harmonic mode locking and multiple pulsing in a ti: sapphire laser," Opt. Express **16**(6), 3686–3692 (2008).
28. S. B. Mirov, I. S. Moskalev, S. Vasilyev, *et al.*, "Frontiers of mid-ir lasers based on transition metal doped chalcogenides," IEEE J. Sel. Top. Quantum Electron. **24**(5), 1–29 (2018).
29. A. Barh, J. Heidrich, B. Alaydin, *et al.*, "Watt-level and sub-100-fs self-starting mode-locked 2.4-μm cr: Zns oscillator enabled by gasb-sesams," Opt. Express **29**(4), 5934–5946 (2021).
30. J. Heidrich, A. Barh, S. L. Camenzind, *et al.*, "Low-noise femtosecond sesam modelocked diode-pumped cr: Zns oscillator," IEEE J. Quantum Electron. **59**(1), 1–7 (2023).
31. M. N. Cizmeciyan, H. Cankaya, A. Kurt, *et al.*, "Kerr-lens mode-locked femtosecond cr 2+: Znse laser at 2420 nm," Opt. Lett. **34**(20), 3056–3058 (2009).
32. N. Tolstik, E. Sorokin, and I. T. Sorokina, "Kerr-lens mode-locked cr: Zns laser," Opt. Lett. **38**(3), 299–301 (2013).
33. S. Vasilyev, I. Moskalev, M. Mirov, *et al.*, "Three optical cycle mid-ir kerr-lens mode-locked polycrystalline cr 2+: Zns laser," Opt. Lett. **40**(21), 5054–5057 (2015).
34. P. Steinleitner, N. Nagl, M. Kowalczyk, *et al.*, "Single-cycle infrared waveform control," Nat. Photonics **16**(7), 512–518 (2022).
35. Y. Wang, F. Fleming, R. A. McCracken, *et al.*, "Hot-isostatic-pressed cr: Znse ultrafast laser at 2.4 μm," Opt. Laser Technol. **154**, 108300 (2022).
36. V. L. Kalashnikov, E. Sorokin, and I. T. Sorokina, "Multipulse operation and limits of the kerr-lens mode-locking stability," IEEE J. Quantum Electron. **39**(2), 323–336 (2003).
37. I. T. Sorokina and K. L. Vodopyanov, *Solid-state mid-infrared laser sources*, vol. 89 (Springer Science & Business Media, 2003).
38. E. Sorokin, N. Tolstik, K. I. Schaffers, *et al.*, "Femtosecond sesam-modelocked cr: Zns laser," Opt. Express **20**(27), 28947–28952 (2012).
39. X. Bu, Y. Shi, J. Xu, *et al.*, "Generation of bound states of pulses in a sesam mode-locked cr: Znse laser," Appl. Phys. B **124**(6), 99 (2018).
40. S. O. Leonov, M. P. Frolov, Y. V. Korostelin, *et al.*, "Bound soliton formation in a sesam mode-locked cr: Znse laser with birefringent plates," Appl. Phys. B **127**(4), 56 (2021).
41. J. Soto-Crespo, N. Akhmediev, V. Afanasjev, *et al.*, "Pulse solutions of the cubic-quintic complex ginzburg-landau equation in the case of normal dispersion," Phys. Rev. E **55**(4), 4783–4796 (1997).
42. J. Soto-Crespo and P. Grelu, "Temporal multi-soliton complexes generated by passively mode-locked lasers," Dissipative Solitons pp. 207–239 (2005).
43. Y. Han, B. Gao, H. Wen, *et al.*, "Pure-high-even-order dispersion bound solitons complexes in ultra-fast fiber lasers," Light: Sci. Appl. **13**(1), 101 (2024).
44. L. Gui, X. Xiao, and C. Yang, "Observation of various bound solitons in a carbon-nanotube-based erbium fiber laser," J. Opt. Soc. Am. B **30**(1), 158–164 (2013).
45. N. Akhmediev and A. Ankiewicz, "Generation of a train of solitons with arbitrary phase difference between neighboring solitons," Opt. Lett. **19**(8), 545–547 (1994).
46. N. Akhmediev, A. Ankiewicz, and J. Soto-Crespo, "Multisoliton solutions of the complex ginzburg-landau equation," Phys. Rev. Lett. **79**(21), 4047–4051 (1997).
47. Q. Ru, N. Lee, X. Chen, *et al.*, "Optical parametric oscillation in a random polycrystalline medium," Optica **4**(6), 617–618 (2017).
48. E. Sorokin, A. Rudenkov, N. Tolstik, *et al.*, "Atmospheric dispersion management in mid-ir mode-locked oscillators," Opt. Express **31**(12), 18790–18798 (2023).
49. A. Rudenkov, V. L. Kalashnikov, E. Sorokin, *et al.*, "High peak power and energy scaling in the mid-ir chirped-pulse oscillator-amplifier laser systems," Opt. Express **31**(11), 17820–17835 (2023).
50. N. Tolstik, E. Sorokin, and I. T. Sorokina, "Graphene mode-locked cr: Zns laser with 41 fs pulse duration," Opt. Express **22**(5), 5564–5571 (2014).
51. N. Tolstik, O. Okhotnikov, E. Sorokin, *et al.*, "Femtosecond cr: Zns laser at 2.35 μm mode-locked by carbon nanotubes," in *Solid State Lasers XXIII: Technology and Devices*, vol. 8959 (SPIE, 2014), pp. 206–211.
52. B. Ortaç, A. Zaviyalov, C. K. Nielsen, *et al.*, "Observation of soliton molecules with independently evolving phase in a mode-locked fiber laser," Opt. Lett. **35**(10), 1578–1580 (2010).
53. D. Zou, Y. Zhang, Y. Song, *et al.*, "Sub-100 fs bound state solitons and period-doubling bifurcations in a mode-locked fiber laser," IEEE Photonics Technol. Lett. **32**(20), 1311–1314 (2020).

Optics EXPRESS

54. B. Fu, J. Li, Z. Cao, *et al.*, "Bound states of solitons in a harmonic graphene-mode-locked fiber laser," Photonics Res. **7**(2), 116–120 (2019).
55. X. Ren, H. Li, W. Chen, *et al.*, "Generation of controllable bound solitons from a thulium–holmium co-doped mode-locked fiber laser," Opt. Fiber Technol. **71**, 102950 (2022).
56. M. Chernysheva, A. Bednyakova, M. Al Araimi, *et al.*, "Double-wall carbon nanotube hybrid mode-locker in tm-doped fibre laser: A novel mechanism for robust bound-state solitons generation," Sci. Rep. **7**(1), 44314 (2017).
57. J. Huang, M. Pang, X. Jiang, *et al.*, "Route from single-pulse to multi-pulse states in a mid-infrared soliton fiber laser," Opt. Express **27**(19), 26392–26404 (2019).
58. Y. Liu, S. Huang, Z. Li, *et al.*, "Phase-tailored assembly and encoding of dissipative soliton molecules," Light: Sci. Appl. **12**(1), 123 (2023).
59. P. Rohrmann, A. Hause, and F. Mitschke, "Solitons beyond binary: possibility of fibre-optic transmission of two bits per clock period," Sci. Rep. **2**(1), 866 (2012).
60. M. Stratmann, T. Pagel, and F. Mitschke, "Experimental observation of temporal soliton molecules," Phys. Rev. Lett. **95**(14), 143902 (2005).
61. A. Barh, B. Ö. Alaydin, J. Heidrich, *et al.*, "High-power low-noise 2-ghz femtosecond laser oscillator at 2.4 μm," Opt. Express **30**(4), 5019–5025 (2022).
62. M. Pang, W. He, X. Jiang, *et al.*, "All-optical bit storage in a fibre laser by optomechanically bound states of solitons," Nat. Photonics **10**(7), 454–458 (2016).
63. F. Leo, S. Coen, P. Kockaert, *et al.*, "Temporal cavity solitons in one-dimensional kerr media as bits in an all-optical buffer," Nat. Photonics **4**(7), 471–476 (2010).